Available online at www.sciencedirect.com
ScienceDirect
Journal of Power Sources 176 (2008) 325–331
JOURNAL OF POWER SOURCES
www.elsevier.com/locate/jpowsour

Effect of equivalent and non-equivalent Al substitutions on the structure and electrochemical properties of $LiNi_{0.5}Mn_{0.5}O_2$

Bin Zhang, Gang Chen *, Ping Xu, Cui Cui Li

Department of Applied Chemistry, Harbin Institute of Technology, Harbin 150001, PR China

Received 9 June 2007; received in revised form 4 October 2007; accepted 6 October 2007
Available online 23 October 2007

Abstract

Pristine, equivalently and non-equivalently Al substituted $LiNi_{0.5}Mn_{0.5}O_2$ materials were prepared by a combination of co-precipitation and solid-state reaction. As shown by XRD and XPS, lattice volume shrinkage of $LiNi_{0.5}(Mn_{0.45}Al_{0.05})O_2$ was attributed to the presence of Ni in both 2+ and 3+, while the lattice volume expansion of $Li(Ni_{0.45}Al_{0.05})Mn_{0.5}O_2$ was caused by lowering the average oxidation state of Mn. Electrochemical performance of $LiNi_{0.5}Mn_{0.5}O_2$ materials can be greatly affected by the change of oxidation states of the transition metals by Al substitution. Non-equivalent substitution of Al for Ni leads to deteriorated discharge performance and cyclic stability due to the reduction of the electrochemical active Ni^{2+} and structure supported Mn^{4+}, while an increase in the amount of Ni^{2+} in $LiNi_{0.5}(Mn_{0.45}Al_{0.05})O_2$ brings obvious improvement of the electrochemical properties. EIS analyses of the electrode materials at pristine and charged states indicate that the poor electrochemical performance of $Li(Ni_{0.45}Al_{0.05})Mn_{0.5}O_2$ material can be ascribed to the higher charge transfer resistance and surface film resistance, and the observed higher current rate capability of $LiNi_{0.5}(Mn_{0.45}Al_{0.05})O_2$ can be understood due to the better charge transfer kinetics.

Keywords: $LiNi_{0.5}Mn_{0.5}O_2$; Al substitution; Layered structure; Electrochemical properties; Electrochemical impedance spectroscopy (EIS)

1. Introduction

The cathode material in the current commercial rechargeable lithium batteries usually is $LiCoO_2$, and many recent reports have been addressed the problem in synthesizing a cheaper, higher capacity, and safer layered cathode material than $LiCoO_2$ [1–3]. Layered lithium nickel manganese oxides are promising, cheap, and non-toxic alternative cathode materials to the commercial $LiCoO_2$ electrode used in Li-ion batteries. Among these materials, $LiNi_{0.5}Mn_{0.5}O_2$ is one of the most attractive, due to its higher specific capacity, lower cost, and excellent thermal stability [4–6]. However, there are some difficulties to be overcomed, in order to be applied in the future, such as uneasy preparation of stoichiometric phases [7], poor rate capacity [8], and cycle instability [9].

It is well known that foreign metal ion doping is an effective way to improve the electrochemical properties of the cathode materials [10]. Some foreign metal ions, such as Co [11,12], Al [13,14], Mg [13], and Ti [7,13,14], have been chosen as the dopants to improve the electrochemical performances of $LiNi_{0.5}Mn_{0.5}O_2$, by equivalent or non-equivalent substitution in terms of charge balance [15]. Kang and Amine [13] used Co, Al, Ti as the dopants to prepare $Li(Ni_{0.475}Mn_{0.475})Co_{0.05}O_2$, $Li(Ni_{0.475}Mn_{0.475})Al_{0.05}O_2$, and $Li(Ni_{0.475}Mn_{0.475})Ti_{0.05}O_2$, and the discharge capacities in the voltage range of 2.8–4.3 V was increased from 120 mAh g^{-1} (with a slight capacity fade up to 40 cycles) to 140, 142, and 132 mAh g^{-1}, respectively (almost no capacity fade was observed). Myung et al. [14] studied Al and Ti doping in $LiNi_{0.5}Mn_{0.5}O_2$ and found that $LiNi_{0.475}Mn_{0.475}Al_{0.05}O_2$ which presents the smallest cation mixing showed the smallest irreversible capacity. However, the effects of different substitutions, equivalent and non-equivalent, by one same metal ion, have not been systematically studied.

In this paper, aluminum was chosen as the doping element due to the equality of its valence as the average valence of nickel and manganese in $LiNi_{0.5}Mn_{0.5}O_2$. And the

* Corresponding author at: No. 92 West Dazhi Street, Nangang District, Harbin 150001, PR China. Tel.: +86 451 86413753; fax: +86 451 86413753.
E-mail address: gchen@hit.edu.cn (G. Chen).

0378-7753/$ – see front matter © 2007 Elsevier B.V. All rights reserved.
doi:10.1016/j.jpowsour.2007.10.043

effects of equivalent substitution ($Li(Ni_{0.475}Mn_{0.475})Al_{0.05}O_2$) and non-equivalent substitution ($Li(Ni_{0.45}Al_{0.05})Mn_{0.5}O_2$, and $LiNi_{0.5}(Mn_{0.45}Al_{0.05})O_2$) on the structural and electrochemical properties of the pristine $LiNi_{0.5}Mn_{0.5}O_2$ were systematically compared by XRD, X-ray photoelectron spectroscopy (XPS), cyclic voltammetry (CV), electrochemical impedance spectroscopy (EIS), and charge–discharge tests.

2. Experimental

2.1. Materials preparation

$LiNi_{0.5}Mn_{0.5}O_2$, $Li(Ni_{0.475}Mn_{0.475})Al_{0.05}O_2$, $Li(Ni_{0.45}Al_{0.05})Mn_{0.5}O_2$, and $LiNi_{0.5}(Mn_{0.45}Al_{0.05})O_2$ samples were synthesized by a combination of co-precipitation and solid-state reaction. Stoichiometric amounts of nickel (II) sulfate and manganese(II) sulfate were dissolved in deionized water. 2 M of NaOH solution and $NH_3{\cdot}H_2O$ (28–30%) were added dropwise into the above solution under severe stirring with argon aerating to keep the oxidation states of Ni and Mn. The mixed hydroxide precipitation was then filtered, washed, and dried overnight at 120 °C. The mixed hydroxide precipitation was then grinded with a required amount of $LiOH{\cdot}H_2O$, $Al(NO_3)_3$, heated at 450 °C for 5 h, and pressed into pellet, followed with calcination at 1000 °C for 24 h in air.

2.2. Materials characterization

The crystallite structures of the prepared samples were determined on a D/max-RC X-ray diffractometer (Rigaku), with a Cu Kα radiation source (λ = 1.5405 Å, 45 kV, 50.0 mA). The 2θ Bragg angles were scanned over a range of 10–80°. The XPS spectra were collected on an American Electronics physical PHI5700ESCA system X-ray photoelectron spectroscope using Al Kα radiation (1486.6 eV). The source was operated at 12.5 kV and the anode power was 250 W. The binding energy (BE) was calibrated with the C 1s peak. Electrochemical impedance spectroscopy (EIS) and cyclic voltammetry (CV) were measured on an electrochemical workstation (CHI 660A). EIS was applied on the electrode at pristine and charged (to 4.6 V, the open circuit voltages (OCV) of $Li(Ni_{0.475}Mn_{0.475})Al_{0.05}O_2$, $Li(Ni_{0.45}Al_{0.05})Mn_{0.5}O_2$, and $LiNi_{0.5}(Mn_{0.45}Al_{0.05})O_2$ are 4.47, 4.42, and 4.45 V, respectively) states in the frequency range of 0.01–100,000 Hz with an applied amplitude of 0.005 V. CV was carried out at a scanning rate of 0.1 mV s^{-1} between 2.7 and 4.7 V (*vs.* Li/Li^+). Charge–discharge performance of the cell was characterized galvanostatically on BTS 5 V/1 mA battery testing system (Shenzhen, China) at different discharge current densities in the potential range of 2.8–4.3 and 2.8–4.6 V (*vs.* Li/Li^+).

2.3. Preparation of lithium batteries

The charge–discharge tests were carried out using the standard CR2025 coin-type cell with a single lithium metal foil anode, a celgard 2300 (polypropylene) as the separator, and a cathode. For the preparation of cathode sheets, a slurry formed by mixing the active material (80 wt%), acetylene black (10 wt%), and binder (10 wt%, polyvinylidene fluoride, PVDF, dissolved in *N*-methyl-2-pyrrolidone, NMP), was coated onto an aluminum current collector. The electrodes were dried under vacuum at 120 °C overnight before punched and weighed. The batteries were assembled in a glove box under a dry and high purity argon atmosphere (99.999%). $LiPF_6$ (battery grade) dissolved in a mixture of ethylene carbonate (EC, battery grade) and dimethyl carbonate (DMC, battery grade) (1:1 w/w) was used as the electrolyte.

3. Results and discussion

3.1. Structure characterization of materials

The powder XRD patterns of $LiNi_{0.5}Mn_{0.5}O_2$, $Li(Ni_{0.475}Mn_{0.475})Al_{0.05}O_2$, $Li(Ni_{0.45}Al_{0.05})Mn_{0.5}O_2$, and $LiNi_{0.5}(Mn_{0.45}Al_{0.05})O_2$ samples are shown in Fig. 1. The diffraction patterns of the four samples were similar, with all the peaks indexable based on the α-$NaFeO_2$-type structure (space group $R\bar{3}m$), suggesting that these materials prepared under our condition are well-crystallized and partial substitution of Al for Mn and/or Ni in $LiNi_{0.5}Mn_{0.5}O_2$ will not change the crystalline structure. The oxygen sublattice in the α-$NaFeO_2$-type structure forms a close-packed face centered at the cubic (fcc) lattice with a distortion in the *c* direction, resulting in clear splitting between the (0 0 6)/(1 0 2) and (1 0 8)/(1 1 0) peaks in the XRD patterns. When this distortion in the *c* direction is absent (or the structure is totally cubic), the (0 0 6)/(1 0 2) and (1 0 8)/(1 1 0) peaks merge into single peaks in the diffraction pattern [16]. A good resolution of the (0 0 6)/(0 1 2) and the (0 1 8)/(1 1 0) reflection pairs are typical of an ideal layered structure [17]. The separation between the (0 0 6)/(0 1 2) peaks as well as the (0 1 8)/(1 1 0) peaks can be distinguished more conveniently in all Al substituted materials, especially for the sample $LiNi_{0.5}(Mn_{0.45}Al_{0.05})O_2$, indicating that substitution of Al for proper amount of Mn can lead to ideal layered structure for $LiNi_{0.5}Mn_{0.5}O_2$ cathode materials.

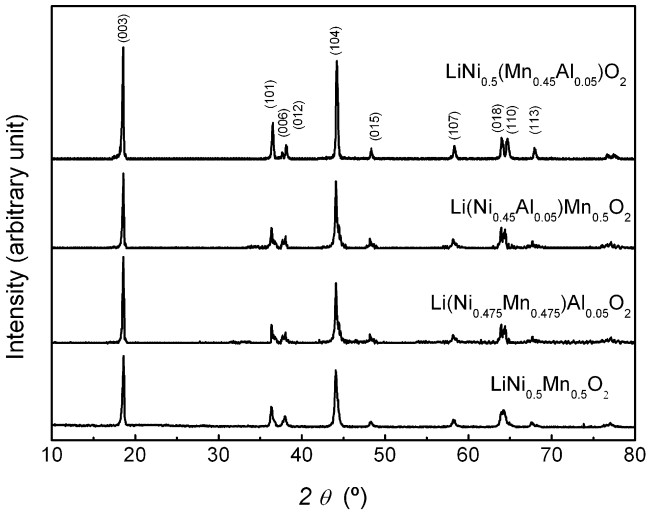

Fig. 1. X-ray diffraction patterns of $LiNi_{0.5}Mn_{0.5}O_2$ and Al substituted samples.

Table 1
Structure parameters of $LiNi_{0.5}Mn_{0.5}O_2$ and Al substituted samples

	$I_{(003)}/I_{(104)}$	a (Å)	c (Å)	V (Å^3)
$LiNi_{0.5}Mn_{0.5}O_2$	1.108	2.8923	14.2502	103.2347
$Li(Ni_{0.475}Mn_{0.475})Al_{0.05}O_2$	1.171	2.8845	14.2227	102.4805
$Li(Ni_{0.45}Al_{0.05})Mn_{0.5}O_2$	1.102	2.8923	14.2980	103.5809
$LiNi_{0.5}(Mn_{0.45}Al_{0.05})O_2$	1.213	2.8815	14.2215	102.2588

Materials Data Jade 5.0 for XRD pattern processing was applied for internal theta calibration, using linear fit and current PDF overlay as references. The calibrated 2θ values were used to calculate the lattice constants a and c, and the calibrated peak intensities were applied to determine the $I_{(003)}/I_{(104)}$ value. Table 1 shows the structure parameters of equivalently and non-equivalently Al substituted and pristine $LiNi_{0.5}Mn_{0.5}O_2$ samples. The intensity ratio of $I_{(003)}/I_{(104)}$ is a sensitive parameter to determine the cation distribution in lattice [18], and the higher this ratio, the lower the degree of the cation mixing. $LiNi_{0.5}(Mn_{0.45}Al_{0.05})O_2$ sample has the highest $I_{(003)}/I_{(104)}$ value, while $Li(Ni_{0.45}Al_{0.05})Mn_{0.5}O_2$ has the smallest, which interprets that substitution of Al for Ni in $LiNi_{0.5}Mn_{0.5}O_2$ results in highest degree of cation mixing, and thus possibly will deteriorate its electrochemical performances. Al introduction in $Li(Ni_{0.475}Mn_{0.475})Al_{0.05}O_2$ and $LiNi_{0.5}(Mn_{0.45}Al_{0.05})O_2$ samples causes shrinkages of both a and c axis and reduction of the lattice volume. However, $Li(Ni_{0.45}Al_{0.05})Mn_{0.5}O_2$ has the same parameter a as pristine $LiNi_{0.5}Mn_{0.5}O_2$, but a larger value of parameter c, leading to lattice volume expansion. The changes of lattice volume of the Al substituted materials seem to be puzzling that the structure parameters of the Al substituted materials do not follow the same rule. Substitution of Al for Mn and (NiMn) causes shrinkage of the lattice volume, on the contrary, substitution of Al for Ni expands the lattice volume. According to Shannon's effective ionic radii [19], the radius of Al^{3+} (0.535 Å) is almost identical to that of Mn^{4+} (0.53 Å, six coordination data) and is smaller than that of Ni^{2+} (0.69 Å). The decreases in the lattice volumes caused by substitution of Al for Mn and (NiMn) should be ascribed to the partial transformation of Ni^{2+} to Ni^{3+} (0.56 Å). When Al^{3+} non-equivalently substitutes Ni^{2+}, the charge compensation from transition metal ions occurs in order to retain the electronic neutrality, which probably gives rise to an increase in the content of the transition metal ions with a low valence by transforming part of Mn^{4+} to Mn^{3+} (0.65 Å) and results in expansion of the lattice volume.

XPS studies are useful in gaining information on the oxidation states of the metal species present in the synthesized lithiated transition metal oxides. XPS measurement was applied in order to determine the oxidation states of the transition metals in these materials due to the debate on the oxidation state of Mn and Ni [6,14]. Fig. 2 shows the Mn 2p and Ni 2p XPS core level spectra for the prepared four samples. The Ni 2p XPS spectrum in Fig. 2(a) shows the characteristic broad satellite peak with the binding energy (BE) at 860.4 eV in all the samples. Such broad satellite peaks are also observed in Ni-containing oxides, such as NiO, $LiNiO_2$, $Li(Ni_{1/3}Co_{1/3}Mn_{1/3})O_2$ and in the spinel, $Li(Mn_{1.5}Ni_{0.5})O_4$ [20–23]. The satellite peak can

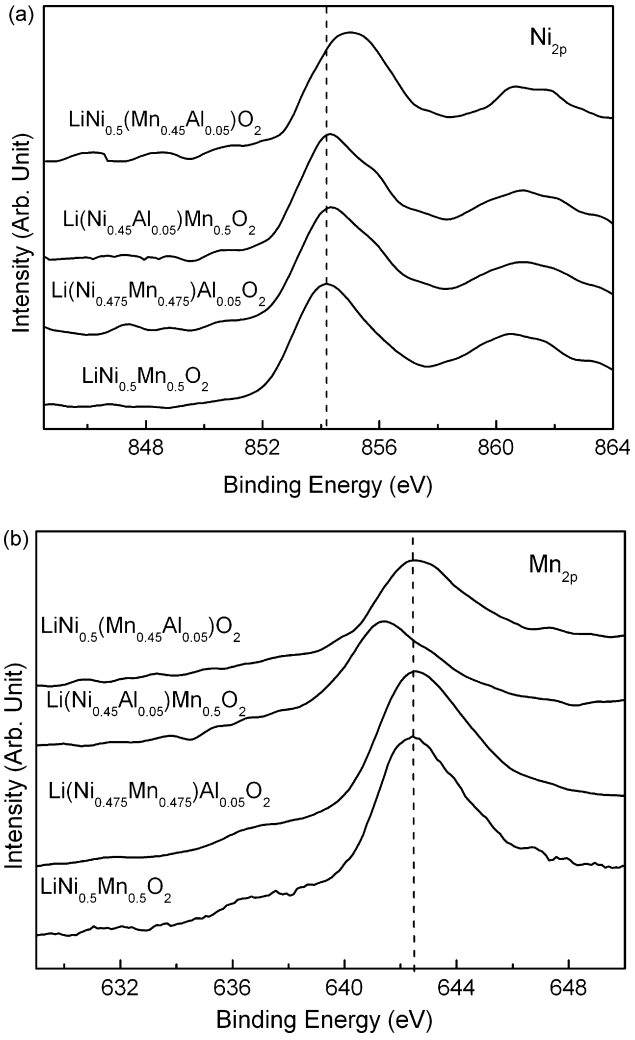

Fig. 2. XPS of (a) Ni 2p and (b) Mn 2p in $LiNi_{0.5}Mn_{0.5}O_2$ and Al substituted samples.

be explained due to the multiple splitting in the energy levels of the Ni-oxides [21,22]. The BE of the center of Ni $2p_{3/2}$ peaks of $LiNi_{0.5}Mn_{0.5}O_2$ is 854.2 eV, which is similar to the BE of Ni^{2+} in NiO, and no shift was found for Al substituted samples except for $LiNi_{0.5}(Mn_{0.45}Al_{0.05})O_2$, whose BE of the center peak is 855.1 eV. The observed higher BE value of $LiNi_{0.5}(Mn_{0.45}Al_{0.05})O_2$ can be attributed to the presence of Ni in both 2+ and 3+ oxidation states, which again reflects that Al substitution for Mn leads to partial transformation of Ni^{2+} to Ni^{3+}.

The Mn 2p XPS spectra of the prepared samples in Fig. 2(b) display that the Mn $2p_{3/2}$ peaks of Al doped samples show no obvious shift except for $Li(Ni_{0.45}Al_{0.05})Mn_{0.5}O_2$, whose Mn $2p_{3/2}$ peak shifts to a lower BE of 641.5 eV. The BE value of Mn $2p_{3/2}$ peak at 642.4 eV is typical for Mn^{4+} oxidation state [24], however, the presence of Mn^{3+} with Mn^{4+} will result in the Mn $2p_{3/2}$ peak shifting to a lower BE. Though the dominant oxidation states of Ni and Mn in pristine and Al substituted $LiNi_{0.5}Mn_{0.5}O_2$ materials are 2+ and 4+, it must be noted that for the non-equivalently substituted $LiNi_{0.5}(Mn_{0.45}Al_{0.05})O_2$, the charge neutrality is achieved by increasing the average valence

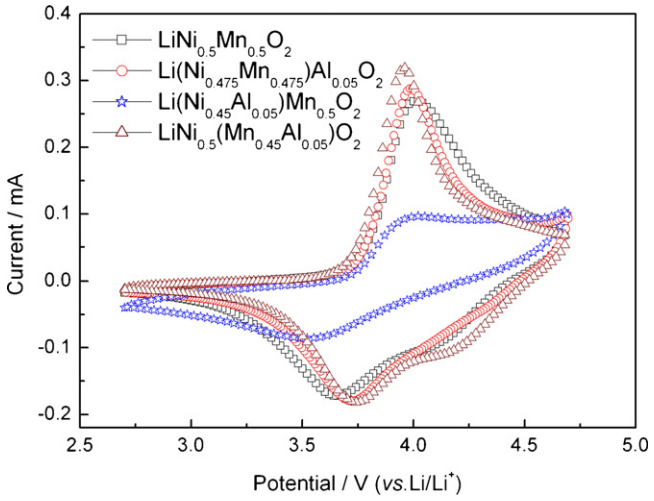

Fig. 3. Cyclic voltammograms of $LiNi_{0.5}Mn_{0.5}O_2$, $Li(Ni_{0.475}Mn_{0.475})Al_{0.05}O_2$, $Li(Ni_{0.45}Al_{0.05})Mn_{0.5}O_2$, and $LiNi_{0.5}(Mn_{0.45}Al_{0.05})O_2$ at a scan rate of 0.1 mV s^{-1}.

of Ni, while the oxidation state of Mn keeping at 4+, which is in agreement with the reported Co non-equivqlent substitution for Mn in $LiNi_{0.5}Mn_{0.5-x}Co_xO_2$ [15]. For $Li(Ni_{0.45}Al_{0.05})Mn_{0.5}O_2$, the charge neutrality is fulfilled by lowering the average valence of Mn, while Ni keeping at 2+. The above results also approve our judgment regarding the reason for the lattice volume shrinkage caused by the non-equivalent substitution of Al for Mn and the lattice volume expansion caused by the non-equivalent substitution of Al for Ni. The analysis of contents of metal ions from XPS also suggests that the molar ratios of the metal elements in the prepared samples are in good agreement with their stoichiometric proportion.

3.2. Electrochemical performance

The cyclic voltammograms (CV) of pristine and Al substituted $LiNi_{0.5}Mn_{0.5}O_2$ samples are shown in Fig. 3. The three Al substituted materials exhibited similar CV to the pristine $LiNi_{0.5}Mn_{0.5}O_2$, with a major sharp oxidizing peak at ca. 4.0 V and broad reducing peak at ca. 3.6 V, which is quite different from that of $LiNiO_2$ that shows three sharp redox peaks caused by three distinct phase transitions [25]. The above observation suggests that no such multi-phase reactions leading to structure degradation during electrochemical cycling are present in $LiNi_{0.5}Mn_{0.5}O_2$ material. Different from other samples, $Li(Ni_{0.45}Al_{0.05})Mn_{0.5}O_2$ sample has obvious reduction current under 3.0 V, which is agreeable with the results of XPS that oxidation state of Mn in $LiNi_{0.5}Mn_{0.5}O_2$, $Li(Ni_{0.475}Mn_{0.475})Al_{0.05}O_2$, and $LiNi_{0.5}(Mn_{0.45}Al_{0.05})O_2$ keeps constantly at 4+, while non-equivalent substitution of Al for Ni lowered the average valence of Mn by transforming part of Mn^{4+} to Mn^{3+} in $LiNi_{0.5}(Mn_{0.45}Al_{0.05})O_2$, because the redox reaction of Mn^{3+}/Mn^{4+} occurs below 3.0 V [26,27], and this can also be explained by increased polarization for this material. The difference between anodic potential φ_{pa} and cathodic potential φ_{pc}, $\Delta\varphi_p = \varphi_{pa} - \varphi_{pc}$, demonstrates the reversibility of the intercalation and deintercalation of lithium ions in the electrode materials, and the lower the value of $\Delta\varphi_p$, the better reversibility of the electrode materials. As shown in Table 2, Al substitution reduces the value of $\Delta\varphi_p$ for $LiNi_{0.5}Mn_{0.5}O_2$ electrode material except for $Li(Ni_{0.45}Al_{0.05})Mn_{0.5}O_2$. The transition-metal layer in $LiNi_{0.5}Mn_{0.5}O_2$ is bi-functional, with Ni^{2+} acting as a double redox-active center [28–30] and Mn^{4+} providing stability to the host structure [31]. The substitution of Al for Ni in $LiNi_{0.5}Mn_{0.5}O_2$ reduces not only the amount of electrochemical active Ni^{2+}, but also the structure-supported Mn^{4+}, which leads to poor electrochemical performance. While the substitution of Al for Mn in $LiNi_{0.5}Mn_{0.5}O_2$ would improve the CV performance of $LiNi_{0.5}Mn_{0.5}O_2$ due to an increase in the amount of Ni^{2+}, as explained by XPS spectra.

Table 2
Potential values of CV peaks for $LiNi_{0.5}Mn_{0.5}O_2$ and Al substituted samples

Samples	φ_{pa} (V)	φ_{pc} (V)	$\Delta\varphi_p$ (V)[a]
$LiNi_{0.5}Mn_{0.5}O_2$	4.01	3.65	0.36
$Li(Ni_{0.475}Mn_{0.475})Al_{0.05}O_2$	3.99	3.72	0.27
$Li(Ni_{0.45}Al_{0.05})Mn_{0.5}O_2$	4.00	3.51	0.49
$LiNi_{0.5}(Mn_{0.45}Al_{0.05})O_2$	3.95	3.75	0.20

[a] $\Delta\varphi_p = \varphi_{pa} - \varphi_{pc}$.

The charge–discharge curves of $LiNi_{0.5}Mn_{0.5}O_2$ and Al substituted materials are shown in Fig. 4. The cells were charged at 10 mA g^{-1} to 4.6 V, and then discharged to 2.8 V at different rate: 10, 100, 200, and 400 mA g^{-1}, respectively. There is only one voltage plateau on both charge and discharge curves, which is consistent with the results in cyclic voltammetry experiments, where only one couple of redox current peaks was observed. As expected, non-equivalent Al substitution of Ni in $LiNi_{0.5}Mn_{0.5}O_2$ material drastically deteriorates the charge–discharge performance at all discharge rates. $LiNi_{0.5}(Mn_{0.45}Al_{0.05})O_2$ has the highest discharge capacity at different discharge rates, and great improvement was also discovered for equivalent Al substitution sample $Li(Ni_{0.475}Mn_{0.475})Al_{0.05}O_2$. The first charge and

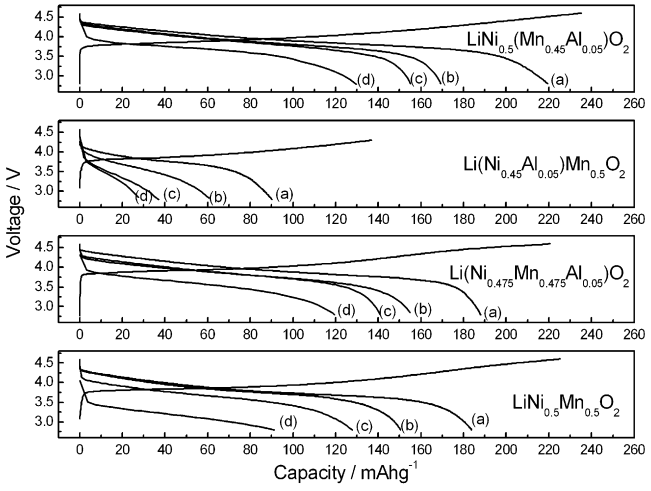

Fig. 4. Charge–discharge curves of $LiNi_{0.5}Mn_{0.5}O_2$ and Al substituted cells. The cells were charged to 4.6 V then discharged at different rate: (a) 10 mA g^{-1}, (b) 100 mA g^{-1}, (c) 200 mA g^{-1}, and (d) 400 mA g^{-1} in the 2.8–4.6 V region.

Table 3
First charge and discharge capacity of $LiNi_{0.5}Mn_{0.5}O_2$ and Al substituted samples at 10 mA g^{-1} charge–discharge rate

	$LiNi_{0.5}Mn_{0.5}O_2$	$Li(Ni_{0.475}Mn_{0.475})Al_{0.05}O_2$	$Li(Ni_{0.45}Al_{0.05})Mn_{0.5}O_2$	$LiNi_{0.5}(Mn_{0.45}Al_{0.05})O_2$
Charge capacity (mAh g^{-1})	225	220	135	234
Discharge capacity (mAh g^{-1})	183	187	90	219
Discharge efficiency (%)	81.33	85.00	66.67	93.59

Discharge efficiency = discharge capacity/charge capacity × 100%.

discharge capacities of $LiNi_{0.5}Mn_{0.5}O_2$ and Al substituted samples at 10 mA g^{-1} charge–discharge rate are shown in Table 3, which shows that best capacity retention was observed for $LiNi_{0.5}(Mn_{0.45}Al_{0.05})O_2$, while $Li(Ni_{0.45}Al_{0.05})Mn_{0.5}O_2$ presents the worst reversibility.

The cyclic stability of $LiNi_{0.5}Mn_{0.5}O_2$ and Al substituted samples was tested under a moderate rate of 40 mA g^{-1} in 2.8–4.3 and 2.8–4.6 V ranges, respectively. As shown in Fig. 5, the sample of non-equivalent Al substitution for Ni, $Li(Ni_{0.45}Al_{0.05})Mn_{0.5}O_2$, displays smallest charge capacities in both cycle tests, while $LiNi_{0.5}(Mn_{0.45}Al_{0.05})O_2$ sample has the best. Discharge capacities of equivalently Al substituted $Li(Ni_{0.475}Mn_{0.475})Al_{0.05}O_2$ and pristine $LiNi_{0.5}Mn_{0.5}O_2$ cycled in a shorter range of 2.8–4.3 V (Fig. 5a) are almost the same. After 40 cycles, no obvious capacity reduction was discovered for all samples in 2.8–4.3 V. For the cells cycled in 2.8–4.6 V (Fig. 5b), the superiority of $LiNi_{0.5}(Mn_{0.45}Al_{0.05})O_2$ and $Li(Ni_{0.45}Al_{0.05})Mn_{0.5}O_2$ can be easily distinguished. Capacity reduction within a narrow range can be found for all four samples at this potential range.

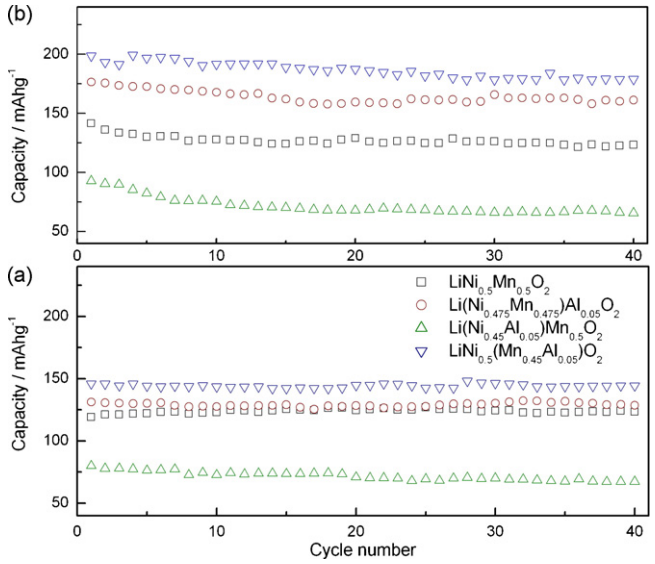

Fig. 5. Cyclic performance of $LiNi_{0.5}Mn_{0.5}O_2$ and Al substituted compounds operated at a current density of 40 mA g^{-1} in (a) 2.8–4.3 V and (b) 2.8–4.6 V.

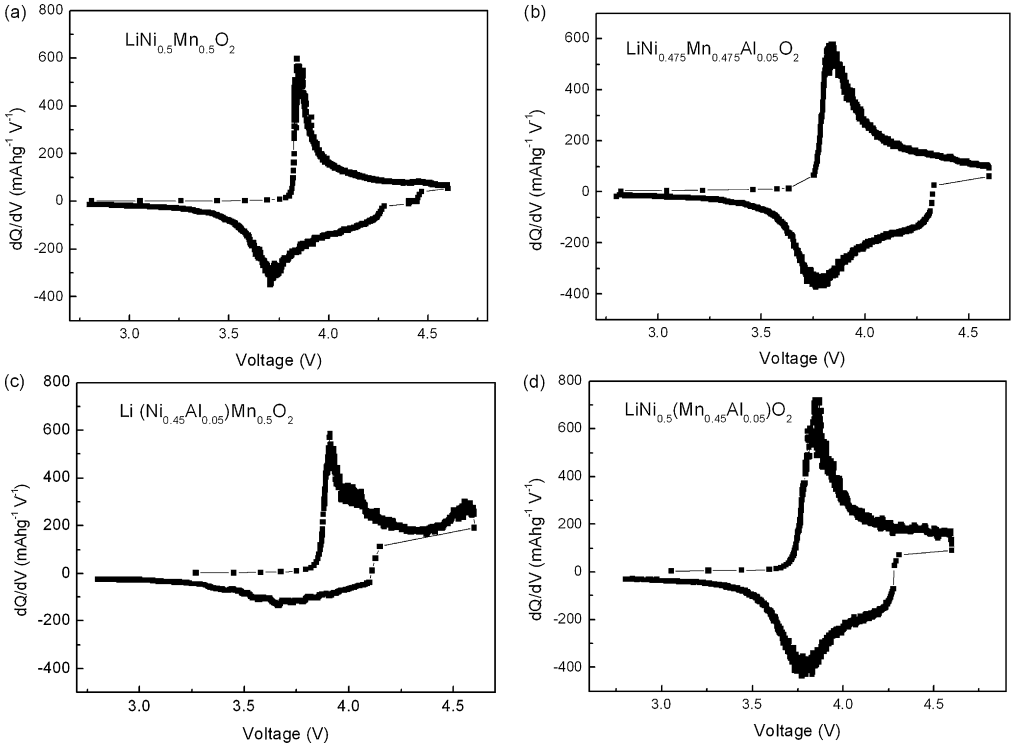

Fig. 6. Differential capacity versus voltage plots of the (a)Li/$LiNi_{0.5}Mn_{0.5}O_2$, (b) Li/$Li(Ni_{0.475}Mn_{0.475})Al_{0.05}O_2$, (c) Li/$Li(Ni_{0.45}Al_{0.05})Mn_{0.5}O_2$, and (d) Li/$LiNi_{0.5}(Mn_{0.45}Al_{0.05})O_2$ cells.

Fig. 6 shows differential capacity curves of $LiNi_{0.5}Mn_{0.5}O_2$ and Al substituted samples at 40 mA g^{-1} charge–discharge rate during first cycle. $LiNi_{0.5}Mn_{0.5}O_2$, $Li(Ni_{0.475}Mn_{0.475})Al_{0.05}O_2$, and $LiNi_{0.5}(Mn_{0.45}Al_{0.05})O_2$ show similar peaks with one oxidation peak at about 3.8 V and one reduction peak at 3.7 V. The smaller difference of the positions between oxidation and reduction peaks indicates the better reversibility of Li intercalation processes in these samples and less capacity reduction during battery cycling [32]. Splitting between charge and discharge peaks of $Li(Ni_{0.45}Al_{0.05})Mn_{0.5}O_2$ sample was much larger than the other three samples. Interestingly, the differential capacity curve of $Li(Ni_{0.5}Al_{0.05})Mn_{0.45}O_2$ shows two peaks during charging, one at about 3.8 V and the other peak at around 4.55 V, which is responsible for the high irreversible capacity in the initial cycle. The latter peak at around 4.55 V is supposed to be characteristic of oxidation of Li_2MnO_3 material and suggests the formation of a solid solution system [7,33]. Lu and Dahn [34] attributed the differential capacity peaks below 3.5 V to participation of Mn ions in the redox reactions in the layered structure, which was not found in our samples.

Electrochemical impedance spectroscopy (EIS) is a powerful tool to identify the kinetics of lithium intercalation/deintercalation into electrodes [35,36]. The lithium intercalation and deintercalation into the cathode materials can be modeled as a multi-step process that involves and reflects a serial nature of several processes occurring during intercalation/deintercalation. The general nature of those models is to explain the Li-ion migration through the surface film, charge-transfer through the electrode/electrolyte interface, and the solid-state diffusion of Li in the compounds. The possible and experimentally visualized processes are (1) a resistive component (R_e) arising from the electrolyte resistance and cell components, (2) the double layer (dl) capacitance of the surface film and the associated impedance (C_{sf} and R_{sf}), (3) the charge transfer (electron transfer) resistance of the intercalation reaction and the capacitance of the double layer (R_{ct} and C_{dl}), and (4) a Warburg contribution (W_o) which is characteristic of the Li ion diffusion through the bulk to the active material [36].

In the present study, EIS tests were performed on the electrodes at pristine state and charged state (to 4.6 V), respectively. As shown in Fig. 7a, the Nyquist plots of the electrodes at the pristine state indicate identical electrochemical mode, with one semicircle at high frequency range and one line at low frequency range, indicating that at the early stage of deintercalation, the kinetics of the electrode process is controlled by the diffusion process in the low frequency region and by the charge transfer in the high frequency region. The observed high frequency semicircle at charged state (see Fig. 7b) which can be assigned to the surface film resistance (R_{sf}) and associated capacitance (C_{sf}), is absent or masked by the medium frequency semicircle in the freshly fabricated cell at pristine state. The semicircle observed in the high frequency domain for all samples in the pristine state is probably related to the lithium ion migration through the interface between the surface layer of the particles and the electrolyte [37,38]. Using the equivalent circuit inset in Fig. 5a, It is calculated that the magnitude of charge transfer resistance

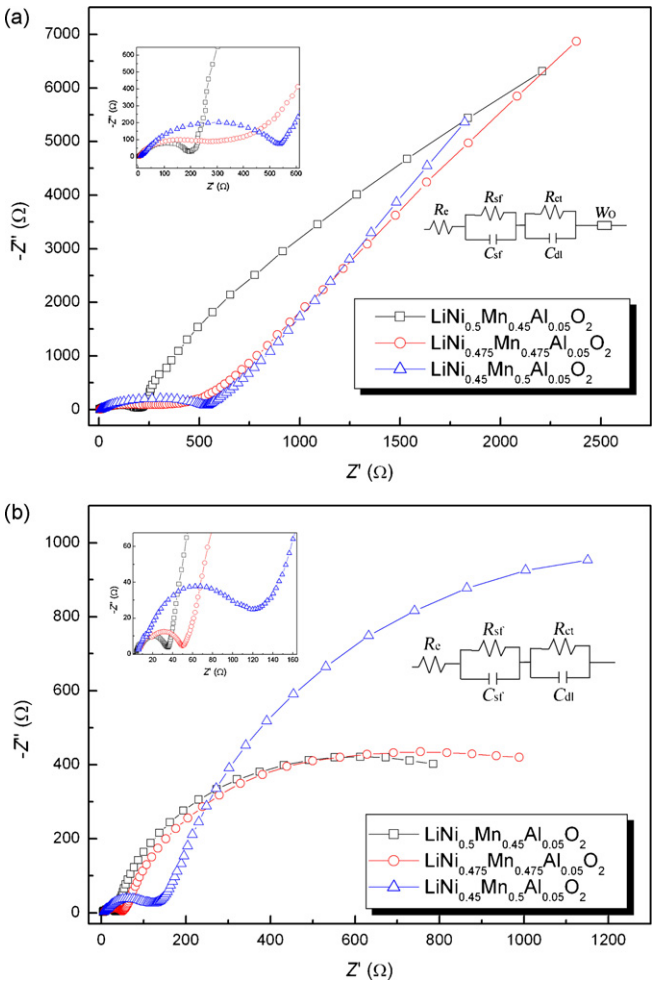

Fig. 7. Nyquist plots of the equivalent and non-equivalent Al substituted $LiNi_{0.5}Mn_{0.5}O_2$ electrode materials at (a) pristine state, and (b) charged state (to 4.6 V). Magnification of the plots in high frequency regions and the equivalent circuit used for simulation are also shown (inset).

(R_{ct}) of the prepared samples follows: $LiNi_{0.5}(Mn_{0.45}Al_{0.05})O_2$ (156.1 Ω) < $Li(Ni_{0.475}Mn_{0.475})Al_{0.05}O_2$ (229.5 Ω) < $Li(Ni_{0.45}Al_{0.05})Mn_{0.5}O_2$ (411.3 Ω). And Li ion diffusion through the bulk to the active material, Warburg contribution (W_o), of $LiNi_{0.5}(Mn_{0.45}Al_{0.05})O_2$ also is most convenient as compared with the other two electrode materials.

EIS spectra of the samples at charged state also show same electrochemical mode (Fig. 7b), with two semicircles, which means that at the end of deintercalation, the electrode kinetics is controlled by the charge transfer contribution. The reason for this periodical change can be understood from the fact that the R_{ct} values increase enormously at the end of deintercalation. The diameter of the lower-frequency semicircle in the plots of the electrode at charged state provides charge-transfer resistance (R_{ct}) associated with the electrochemical process. As simulated with the equivalent circuit inset in Fig. 7b, the values of R_{ct} at charged state for the prepared samples follow the same sequence as that at pristine state, that is, $LiNi_{0.5}(Mn_{0.45}Al_{0.05})O_2$ had the minimum value of R_{ct} (811.9 Ω) at the end of deintercalation, and $Li(Ni_{0.45}Al_{0.05})Mn_{0.5}O_2$ had the largest R_{ct} (1976.1 Ω). This may be caused by differences in the nature

of surface film covering these compounds even though we have used identical cell parameters (electrode thickness, area, and process conditions) for all the systems. The lithiation process with $LiNi_{0.5}(Mn_{0.45}Al_{0.05})O_2$ might have changes not only the morphology of the particle, but also its electronic structure, with a more active surface facilitating easy charge transfer. High frequency semicircles at the charged state are not clearly seen due to the large Z' values of the low frequency semicircles. From the inset magnification in Fig. 7b, the diameters of the high frequency semicircles have the same variation as that at low frequency, indicating that $Li(Ni_{0.45}Al_{0.05})Mn_{0.5}O_2$ has the largest surface film resistance (R_{sf}) at charged state (the end of deintercalation). The R_{sf} may not have an influential role in the electrode kinetics for a single charge or discharge cycle, however, the production of surface film on the electrode on repeated charge–discharge cycling may influence the performance of the electrode material. The nature of surface film, which covers the active mass, may provide a measure of its particle to particle contact. A mass deposition of the surface film on the electrode surface may end up as a destructive film, which would slow down the electrode kinetics and hence its performance [35,39,40]. Thus, the poor charge–discharge performance of $Li(Ni_{0.45}Al_{0.05})Mn_{0.5}O_2$ material can be attributed by the higher charge transfer resistance together with the surface film resistance, and the observed higher current rate capability of $LiNi_{0.5}(Mn_{0.45}Al_{0.05})O_2$ can be understood as due to the better charge transfer kinetics.

4. Conclusion

Pristine, equivalently and non-equivalently Al substituted $LiNi_{0.5}Mn_{0.5}O_2$ materials were prepared by a combination of co-precipitation and solid-state reaction. The effect of equivalent and non-equivalent Al substitutions on the structure and electrochemical properties of $LiNi_{0.5}Mn_{0.5}O_2$ was systematically studied in this paper. Lattice volume changes of Al substituted $LiNi_{0.5}Mn_{0.5}O_2$ materials can be attributed to the transformation of the oxidation states of the transition metals, Ni and Mn, which further greatly affected the electrochemical performance of $LiNi_{0.5}Mn_{0.5}O_2$ materials. Non-equivalent substitution of Al for Ni leads to deteriorated discharge performance and cyclic stability due to the reduction of the electrochemical active Ni^{2+} and structure supported Mn^{4+}, while an increase in the amount of Ni^{2+} in $LiNi_{0.5}(Mn_{0.45}Al_{0.05})O_2$ brings obvious improvement of the electrochemical properties. Improved electrochemical performances were also discovered for the equivalently Al substituted sample, $Li(Ni_{0.475}Mn_{0.475})Al_{0.05}O_2$. Substitution of Al for Ni leads to higher charge transfer resistance at both pristine and charged state and thus poorer electrochemical performance, while the observed higher current rate capability of $LiNi_{0.5}(Mn_{0.45}Al_{0.05})O_2$ can be ascribed to the better charge transfer kinetics.

Acknowledgements

This work was supported by National Science Foundation of China (Project No. 20571019). The Project was sponsored by SRF for ROCS, HLJ (LC06C13) and by Program of Harbin Subject Chief Scientist.

References

[1] A.R. Armstrong, P.G. Bruce, Nature 381 (1996) 499.
[2] J. Bréger, N. Dupré, P.J. Chupas, P.L. Lee, T. Proffen, J.B. Parise, C.P. Grey, J. Am. Chem. Soc. 127 (2005) 7529.
[3] X.Q. Yang, J. McBreen, W.S. Yoon, M. Yoshio, H.Y. Wang, K. Fukuda, T. Umeno, Electrochem. Commun. 4 (2002) 649.
[4] M.E. Spahr, P. Novak, O. Hass, R. Nesper, J. Power Sources 68 (1997) 629.
[5] K. Kang, Y.S. Meng, J. Bréger, C.P. Grey, G. Ceder, Science 311 (2006) 977.
[6] Z. Lu, L.Y. Beaulieu, R.A. Donaberger, C.L. Thomas, J.R. Dahn, J. Electrochem. Soc. 149 (2002) A778.
[7] D.-C. Li, T. Muta, H. Noguchi, J. Power Sources 135 (2004) 262.
[8] B.L. Cushing, J.B. Goodenough, Solid State Sci. 4 (2002) 1487.
[9] S.H. Na, H.S. Kim, S.I. Moon, Electrochim. Acta 50 (2004) 449.
[10] R. Koksbang, J. Barker, H. Shi, M.Y. Saidi, Solid State Ionics 84 (1996) 1.
[11] D.-C. Li, H. Noguchi, M. Yoshio, Electrochim. Acta 50 (2004) 427.
[12] D.-C. Li, Y. Sasaki, M. Kageyama, K. Kobayakawa, Y. Sato, J. Power Sources 148 (2005) 85.
[13] S.H. Kang, K. Amine, J. Power Sources 119–121 (2003) 150.
[14] S.-T. Myung, S. Komaba, N. Hirosaki, K. Hosoya, N. Kumagai, J. Power Sources 146 (2005) 645.
[15] D.-C. Li, Y. Sasaki, K. Kobayakawa, Y. Sato, Electrochim. Acta 51 (2006) 3809.
[16] Y. Gao, M.V. Yakovleva, W.B. Ebner, Electrochem. Solid State Lett. 1 (1998) 117.
[17] R.J. Gummow, M.M. Thackeray, W.I.F. David, S. Hull, Mater. Res. Bull. 27 (1992) 327.
[18] T. Ohzuku, A. Ueda, M. Nagayama, J. Electrochem. Soc. 140 (1993) 1862.
[19] R.D. Shannon, Acta Crystallogr. A 32 (1976) 751.
[20] K.M. Shaju, G.V. Subba Rao, B.V.R. Chowdari, Electrochim. Acta 48 (2002) 145.
[21] A.F. Carley, S.D. Jackson, J.N. O'Shea, M.W. Roberts, Surf. Sci. 440 (1999) L868.
[22] K. Amine, H. Tukamoto, H. Yasuda, Y. Fujita, J. Electrochem. Soc. 143 (1996) 1607.
[23] A.N. Mansour, Surf. Sci. Spectra 3 (1996) 279.
[24] K.M. Shaju, G.V. Subba Rao, B.V.R. Chowdari, Electrochim. Acta 48 (2003) 1505.
[25] W. Li, J.N. Reimers, J.R. Dahn, Solid State Ionics 67 (1993) 123.
[26] J.M. Paulsen, C.L. Thomas, J.R. Dahn, J. Electrochem. Soc. 147 (2000) 861.
[27] K.M. Shaju, G.V.S. Rao, B.V.A. Chowdari, Electrochem. Commun. 4 (2002) 633.
[28] Z. Lu, D.D. MacNeil, J.R. Dahn, Electrochem. Solid State Lett. 4 (2001) A191.
[29] J. Reed, G. Ceder, Electrochem. Solid State Lett. 5 (2002) A145.
[30] J.M. Paulsen, J.R. Dahn, J. Electrochem. Soc. 147 (2000) 2478.
[31] M.M. Thackeray, Prog. Solid State Chem. 25 (1997) 1.
[32] O.A. Shlyakhtin, S.H. Choi, Y.S. Yoon, Y.J. Oh, J. Power Sources 141 (2005) 122.
[33] J.M. Kim, S. Tsuruta, N. Kumagai, Electrochem. Commun. 9 (2007) 103.
[34] Z. Lu, J.R. Dahn, J. Electrochem. Soc. 149 (2002) A815.
[35] M.D. Levi, K. Gamolsky, D. Aurbach, U. Heider, R. Oesten, Electrochim. Acta 45 (2000) 1781.
[36] K.M. Shaju, G.V. Subba Rao, B.V.R. Chowdari, J. Electrochem. Soc. 150 (2003) A1.
[37] D. Aurbach, M. Levi, E. Levi, H. Teller, B. Markovsky, G. Salitra, U. Heider, J. Electrochem. Soc. 145 (1998) 3024.
[38] M. Levi, G. Salitra, B. Markovsky, H. Teller, D. Aurbach, L. Heider, J. Electrochem. Soc. 146 (1999) 1279.
[39] A. Ueda, T. Ohzuku, J. Electrochem. Soc. 141 (1999) 2010.
[40] N. Yabuuchi, T. Ohzuku, J. Power Sources 119–121 (2003) 171.